

High energy cosmic ray physics with underground muons in MACRO.

I. Analysis methods and experimental results

M. Ambrosio,¹² R. Antolini,⁷ G. Auriemma,^{14,*} R. Baker,¹¹ A. Baldini,¹³ G. C. Barbarino,¹² B. C. Barish,⁴ G. Battistoni,^{6,†} R. Bellotti,¹ C. Bemporad,¹³ P. Bernardini,¹⁰ H. Bilokon,⁶ V. Bisi,¹⁶ C. Bloise,⁶ T. Bosio,⁷ C. Bower,⁸ S. Bussino,¹⁴ F. Cafagna,¹ M. Calicchio,¹ D. Campana,¹² M. Carboni,⁶ M. Castellano,¹ S. Cecchini,^{2,‡} F. Cei,^{13,§} V. Chiarella,⁶ A. Corona,¹⁴ S. Coutu,¹¹ G. De Cataldo,¹ H. Dekhissi,^{2,||} C. De Marzo,¹ I. De Mitri,⁹ M. De Vincenzi,^{14,¶} A. Di Credico,⁷ O. Erriquez,¹ R. Fantini,² C. Favuzzi,¹ C. Forti,⁶ P. Fusco,¹ G. Giacomelli,² G. Giannini,^{13,**} N. Giglietto,¹ M. Goretti,^{4,14} M. Grassi,¹³ A. Grillo,⁷ F. Guarino,¹² P. Guarnaccia,¹ C. Gustavino,⁷ A. Habig,⁸ K. Hanson,¹¹ A. Hawthorne,⁸ R. Heinz,⁸ J. T. Hong,³ E. Iarocci,^{6,††} E. Katsavounidis,⁴ E. Kearns,³ S. Kyriazopoulou,⁴ E. Lamanna,¹⁴ C. Lane,⁵ D. S. Levin,¹¹ P. Lipari,¹⁴ N. P. Longley,¹⁷ M. J. Longo,¹¹ G. Mancarella,¹⁰ G. Mandrioli,² A. Margiotta-Neri,² A. Marini,⁶ D. Martello,¹⁰ A. Marzari-Chiesa,¹⁶ M. N. Mazziotta,¹ D. G. Michael,⁴ S. Mikheyev,^{7,‡‡} L. Miller,⁸ P. Monacelli,⁹ T. Montaruli,¹ M. Monteno,¹⁶ S. Mufson,⁸ J. Musser,⁸ D. Nicoló,^{13,§} R. Nolty,⁴ C. Okada,³ C. Orth,³ G. Osteria,¹² O. Palamara,¹⁰ S. Parlari,⁷ V. Patera,^{6,††} L. Patrizii,² R. Pazzi,¹³ C. W. Peck,⁴ S. Petrerá,¹⁰ P. Pistilli,¹⁰ V. Popa,^{2,§§} A. Rainó,¹ J. Reynoldson,⁷ M. Ricciardi,¹⁰ F. Ronga,⁶ U. Rubizzo,¹² A. Sanzgeri,¹⁵ F. Sartogo,¹⁴ C. Satriano,^{14,*} L. Satta,^{6,††} E. Scapparone,⁷ K. Scholberg,⁴ A. Sciubba,^{6,††} P. Serra-Lugaresi,² M. Severi,¹⁴ M. Sitta,¹⁶ P. Spinelli,¹ M. Spinetti,⁶ M. Spurio,² R. Steinberg,⁵ J. L. Stone,³ L. R. Sulak,³ A. Surdo,¹⁰ G. Tarlé,¹¹ V. Togo,² V. Valente,⁶ C. W. Walter,⁴ and R. Webb¹⁵

(MACRO Collaboration)

¹*Dipartimento di Fisica dell'Università di Bari and INFN, 70126 Bari, Italy*

²*Dipartimento di Fisica dell'Università di Bologna and INFN, 40126 Bologna, Italy*

³*Physics Department, Boston University, Boston, Massachusetts 02215,*

⁴*California Institute of Technology, Pasadena, California 91125,*

⁵*Department of Physics, Drexel University, Philadelphia, Pennsylvania 19104*

⁶*Laboratori Nazionali di Frascati dell'INFN, 00044 Frascati (Roma), Italy*

⁷*Laboratori Nazionali del Gran Sasso dell'INFN, 67010 Assergi (L'Aquila), Italy*

⁸*Departments of Physics and of Astronomy, Indiana University, Bloomington, Indiana 47405*

⁹*Dipartimento di Fisica dell'Università dell'Aquila and INFN, 67100 L'Aquila, Italy*

¹⁰*Dipartimento di Fisica dell'Università di Lecce and INFN, 73100 Lecce, Italy*

¹¹*Department of Physics, University of Michigan, Ann Arbor, Michigan 48109*

¹²*Dipartimento di Fisica dell'Università di Napoli and INFN, 80125 Napoli, Italy*

¹³*Dipartimento di Fisica dell'Università di Pisa and INFN, 56010 Pisa, Italy*

¹⁴*Dipartimento di Fisica dell'Università di Roma "La Sapienza" and INFN, 00185 Roma, Italy*

¹⁵*Physics Department, Texas A&M University, College Station, Texas 77843*

¹⁶*Dipartimento di Fisica Sperimentale dell'Università di Torino and INFN, 10125 Torino, Italy*

¹⁷*Swarthmore College, Swarthmore, Pennsylvania 19081*

(Received 3 September 1996; revised manuscript received 5 February 1997)

In this paper, the first of a two-part work, we present the reconstruction and measurement of muon events detected underground by the MACRO experiment at Gran Sasso ($E_\mu \geq 1.3$ TeV in atmosphere). The main aim of this work is to discuss the muon multiplicity distribution as measured in the detector. The data sample analyzed consists of 4.4×10^6 muon events, of which $\sim 263\,000$ are multiple muons, corresponding to a total live time of 5850 h. In this sample, the observed multiplicities extend above $N_\mu = 35$, with intermuon separations up to 50 m and beyond. Additional complementing measurements, such as the inclusive muon flux, the angular distribution, and the muon separation distribution (decoherence), are also included. The physical interpretation of the results presented here is reported in the following companion paper. [S0556-2821(97)00615-2]

PACS number(s): 13.85.Tp, 96.40.De, 96.40.Tv, 98.70.Sa

*Also at Università della Basilicata, 85100 Potenza, Italy.

†Also at INFN Milano, 20133 Milano, Italy.

‡Also at Istituto TESRE/CNR, 40129 Bologna, Italy.

§Also at Scuola Normale Superiore di Pisa, 56010 Pisa, Italy.

||Also at Faculty of Sciences, University Mohamed I, B.P. 424 Oujda, Morocco.

¶Also at Dipartimento di Fisica, Università di Roma Tre, Roma, Italy.

**Also at Università di Trieste and INFN, 34100 Trieste, Italy.

††Also at Dipartimento di Energetica, Università di Roma, 00185 Roma, Italy.

‡‡Also Institute for Nuclear Research, Russian Academy of Science, 117312 Moscow, Russia

§§Also Institute of Gravity and Space Sciences, 76900 Bucharest, Romania.

I. INTRODUCTION

The measurement of the primary composition at high energies ($\geq 10^{14}$ eV) and of its possible variations around the steepening of the primary spectrum (the “knee,” at about 2×10^{15} eV), is one of the main experimental problems in cosmic ray physics. Because of the low fluxes, measurements must be indirect, i.e., through the study of the extensive air shower (EAS) components. Measurements are then sensitive not only to the primary spectrum and composition, but also to the interaction properties. The analysis of muon events detected deep underground is one of the most interesting tools for the indirect study of primary composition, since it can be shown that the muon multiplicity, for a given energy threshold of muons, is sensitive to both the energy and mass number of the primary particle [1].

The analysis of these events is complicated by the finite size of the detector, which in general samples only part of an event. At the depth of the Gran Sasso underground laboratory (in average about 3800 hg/cm^2), the typical radius which encloses a multimMuon event is of the order of 10 m. However, the MACRO detector [2] allows measurements of multiple muons to an accuracy (both statistical and systematic) well beyond that of all previous underground experiments. In fact, the horizontal area of MACRO useful for vertical muon tracking is $12 \text{ m} \times 76.5 \text{ m}$. Vertically, the apparatus is 9 m high and consists of a lower part (4.8 m high) and an upper part (called “attico,” added later in time). For the analysis presented here, only the lower part has been used. It allows muon tracking in 10 horizontal planes, almost equally spaced, with point resolution of the order of 1 cm. Zenith angles up to 60° are considered in the measurement presented here, and this allow an acceptance for downgoing muons of $3100 \text{ m}^2 \text{ sr}$. This large dimension allows collection of high multiplicity events with a considerable acceptance and with very little bias introduced into their lateral distribution. This point is fundamentally important in the interpretation of data collected by a finite area detector. The MACRO detector accumulates underground muon data at the rate of $\approx 6.6 \times 10^6$ events/live yr, of which $\approx 4.0 \times 10^5$ exhibit multiple muon tracks and $\approx 1.6 \times 10^3$ are of multiplicity ten or more.

The main topic addressed in this work is the study of the multiplicity distribution. The analyzed sample corresponds to a total live time of 5850 h, i.e., $\sim 4.4 \times 10^6$ muon events, of which $\sim 263\,000$ are multiple muons. Additional analyses are also reported. They address other topics which can be effectively probed by a powerful deep underground detector and include the surface muon flux, angular distribution, and muon track separation. These studies, aside from their intrinsic interest, improve our understanding of the fundamental processes which govern the cascade development in the atmosphere and their modeling, thus reinforcing confidence on the composition results. Combined with our ever improving ability to model cosmic ray showers, the data collected by MACRO represent a unique opportunity to expand our understanding of cosmic ray physics.

Our first results on primary composition, muon track separation in multiple muons, and on the inclusive muon flux have been already published [3–5]. Here we present a complete and detailed discussion on the muon measurements per-

formed in MACRO, including all updated results. Our aim is to include all parts of analysis inside a global context, and to emphasize their underlying coherence, in order to reinforce our primary composition results. Our understanding of the experimental data allows a real composition measurement from the underground muon analysis alone, rather than a simpler test of preexisting models, as done previously [3]. Of course, as in all indirect measurements in cosmic ray physics, the final interpretation is unavoidably dependent on the model adopted to describe the secondary production and transport. Therefore a particular effort in understanding model systematics has been undertaken.

Due to the scope of this work, we present it in two parts. In this first part, we describe the experimental methods and show the experimental data, while the second work [6] is dedicated to the physical interpretation of the results and discusses the newly developed analysis method and the cosmic ray cascade simulations used as reference.

After a description of the MACRO experiment given in Sec. II, where we shall address primarily the tracking system, in Sec. III, the detector simulation is presented. The characteristics of the Gran Sasso rock are summarized in Sec. IV. Section V is dedicated to the experimental results, with particular emphasis to the muon multiplicity distribution; the concluding remarks are given in Sec. VI.

II. MACRO AND THE BASIC FEATURES OF THE TRACKING DETECTORS

The MACRO detector, detailed elsewhere [2], is located in Hall B of the Gran Sasso underground laboratory. Briefly, it is a large area detector equipped with streamer tube chambers, liquid scintillator tanks, and track-etch detectors arranged in a modular structure (supermodules). Each of the six supermodules is $12 \text{ m} \times 12 \text{ m} \times 9 \text{ m}$ in size and consists of a 4.8 m high lower level filled with rock absorber and a 4.2 m high hollow upper level. In this paper, only data from the lower level of the apparatus are included and so only this will be described further. Muon physics analysis has been performed from data samples collected with any of the trigger systems based on scintillators and streamer tubes, separately or in combination, and we refer to [2] for the detailed description.

The tracking is performed with the streamer tubes, which are distributed on 10 horizontal planes, separated by $\sim 60 \text{ g cm}^{-2}$ of CaCO_3 (limestone rock) absorbers, and on 6 planes on each vertical wall. The streamer tubes have a square cross section of $3 \times 3 \text{ cm}^2$, and are 12 m long. For each plane two coordinates are digitally read out, the wire view and the pickup strip view. Pickup aluminum strips are 3 cm wide and are aligned at a stereo angle of 26.5° with respect to the streamer tubes. Spatial resolution depends on the granularity and performance of both wire and pickup strip views. More precisely, the localization of the track is defined by the centroid of a cluster, which is the group of tracking elements fired while the particle crosses a plane. This arrangement gives a spatial resolution of the order of 1–2 cm in both views, corresponding to an intrinsic angular resolution of 0.2° for muons crossing ten horizontal planes.

In Fig. 1 we show as an example one of our multiple muon events, as seen by the on-line display of the experi-

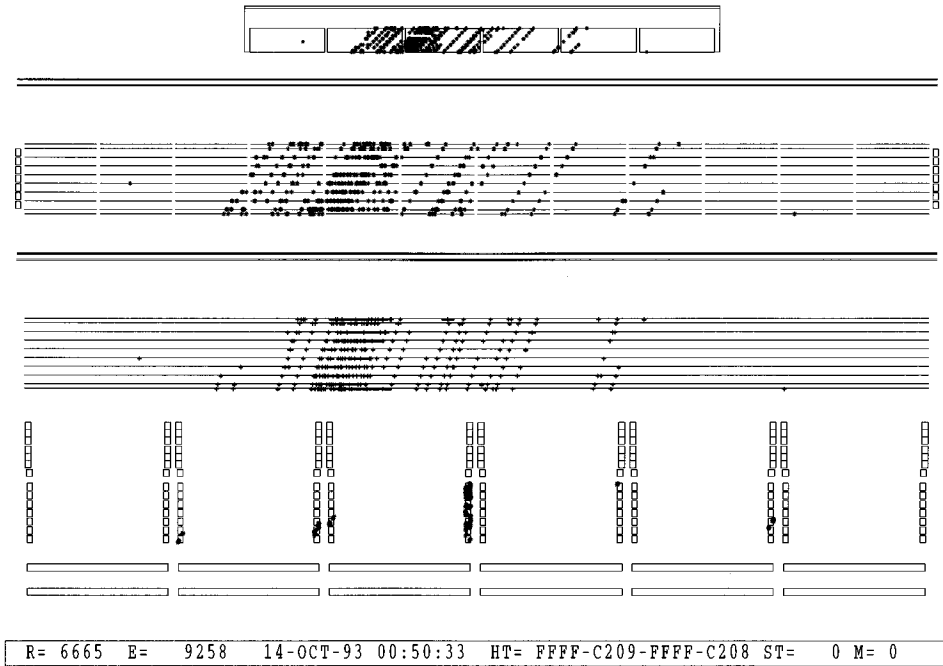


FIG. 1. Example of a multiple muon event as presented by the on-line event display of the experiment. The top part of the plot gives a global size view of the detector, while the projective views of the tracking planes are displayed in detail in the central part: wire above, strips below. In the bottom region, the lateral views (unessential for the analysis presented here) are displayed. This is an example of a high multiplicity event for which visual scanning is necessary (using magnified views), since not all the tracks missing in a detector module, just at the core of event, hits are clearly missing in the bottom plane and in the fourth plane from above; this is due to a temporary failure in the readout chain, which, however, does not affect the efficiency of event recognition and multiplicity evaluation.

ment. The top part of the figure gives a global view of the detector, while the two projective views of the horizontal tracking planes are displayed in the central part (wires above and strips below), together with the additional views from the lateral planes (in the bottom part of the figure).

Tracks on the different views can be associated in space in the majority of events, depending upon the spatial separation and multiplicity. This is automatically achieved when two tracks pass through separate detector modules. When they are in the same module, matching of hit wires and strips on the same detector plane is accomplished by taking advantage of the stereo angle of the strips with respect to the wires. In a fraction of cases the track pattern correspondence between the two views is also used. The unique association of the tracks permits the reconstruction of the distance between muons from their projective views. In the following subsections, we give a description of the muon pattern recognition and tracking adopted in MACRO.

A. Muon pattern recognition and tracking

Muon recognition is based on the search for a minimum number (generally 4) of aligned clusters. An error for each position, derived from the cluster width, is used to discard large and not well-aligned clusters (depending on the event topology).

Pattern recognition is performed at a first level on the wire and strip views separately. At a second level the requirement to obtain a complete matching between the two projective views is invoked. This second level condition effectively rejects accidental noise patterns, generally constituted by the

minimum number of aligned clusters. In case of longer tracks it signals the presence of spurious clusters associated to the main track. These are from secondaries, mostly δ rays, associated with the muon track and originated by the muon interactions in the apparatus, or in the rock. In this last case, the clusters are localized in the outermost planes of the detector.

A conservative procedure is used to search for muon patterns, mostly dictated by the need to handle huge amounts of data taken during a very long period of data acquisition, and possibly affected by different run conditions. The clusters are grouped by plane and all the possible pairs of pivot points are processed by looking at the resulting set of associated, aligned clusters. The first pivot points belong to the outermost planes and they correspond to the best defined direction. The direction defined by the pivot clusters is compared to the one determined by the clusters in the other planes and if they coincide within a specified tolerance, an additional cluster enters the cluster set of the track candidate. At the end the candidates are compared to each other to select the subsample of tracks made by independent clusters. The final candidate is the track having the largest number of clusters, and in case of parity, is the track whose direction is better defined, having the smallest χ^2 value. Those clusters are linearly fitted to compute the direction and the intersection point with the wire/strip axis.

The high streamer tube efficiency helps to avoid degradation of the angular resolution due to spurious clusters. Those hits appearing after three empty planes are rejected, unless the track is verified to be in the region between two contigu-

ous modules where the dead space can account for such a topology.

The above procedure is fully efficient in locating the muons firing the minimum number of requested planes. Furthermore, the requirement to collect at least four hit planes almost completely eliminates the fake candidates.

Less straightforward is the approach used to recognize multiple-muon patterns. It takes into account different pieces of information and establishes a hierarchy between them based on the relative occurrence of conditions. When more than one candidate muon is found, the analysis of the track clusters selects one or more groups of candidates. The candidates can share at most one cluster so that if they intersect they must also define different directions. The most likely bundle is chosen on the assumption that it contains the greatest number of long, well-defined and parallel tracks. The longest track, having the most consistent combination of small clusters, is used to compare the direction of the others and if they are parallel the compared track enters the candidate muon group. If more than one group is selected in this way, the number of tracks belonging to the bundle, the number of clusters per track, and the track length are used to choose the best multimMuon candidate. Once the most likely muon group has been chosen, the procedure searches for other independent, nonparallel tracks (pion candidates) to be associated to the main group and to complete the pattern analysis.

As for singles, in the case of muon groups the procedure first considers the two views separately and then it analyzes the clusters in the bundle searching for the most likely counterpart in the other projective view. The counterpart is isolated by the track position, the track length, and the correspondence of hit and/or nonhit planes in the two views.

The tracking procedure gives for each event the number of tracks in the wire and the strip views, and for each track supplies the slopes and the intercepts together with their errors, the χ^2 , the list of the clusters belonging to its trajectory, and the minimum set of counterpart tracks in the other view, isolated by the analysis described above.

B. Space and angular accuracy of the tracking system

The cluster width distribution affects the spatial accuracy obtained in the stereo view. Such a distribution is primarily affected by the induction of the streamer signal on adjacent strips. This depends on the detector design, gas mixture, and on the electronic threshold of the readout elements. Moreover, track reconstruction is affected by muon interactions just outside and within the apparatus. For example, e.m. processes leaving energy deposits in the streamer tube units near a cell that the particle crosses, can enlarge the cluster width. To give an idea of the cross section of these interactions, we note that particles detected in MACRO are mostly atmospheric muons with an average residual energy of about 280 GeV. The threshold energy for a vertical underground muon to cross MACRO is about 1.5 GeV. Only a negligible fraction (less than 0.5%) of downward-going muons stops or undergoes large multiple scattering in the detector. A straight line fit is therefore well suited to identify muons, and we require at least four aligned hits in different horizontal planes to define a muon track, in all but few particular cases. The

average cluster widths have been measured to be 4.5 cm in the wire and 8.96 cm in the strip view, corresponding to a mean occupancy of 1.45 and 2.75 elements, respectively.

Space resolution achieved without any selection on the tracks is $\sigma_w = 1.1$ cm, and $\sigma_s = 1.6$ cm. These figures are the residuals obtained by subtracting the cluster centers from the position of the straight line passing through the other hits belonging to the track.

For each hit element the actual coordinate is assumed to be uniformly distributed within the cluster width. The angular resolution depends on the cluster widths and on the track length. The average errors on the projected angles with respect to the vertical, θ_w and θ_s , are $\sigma_{\theta_w} = 0.14^\circ$, $\sigma_{\theta_s} = 0.29^\circ$ [2,7].

III. DETECTOR SIMULATION

The modularity of MACRO and the standard tools provided by the CERN package GEANT [8] have been used to simulate in detail the response of the apparatus.

Plastic boxes filled with liquid scintillator, plastic streamer tubes filled with gas and iron boxes filled with Gran Sasso rock, are the basic elements used to describe the structures of the full detector. The data base resulting from the geometrical survey of the apparatus has been used to achieve the maximum possible accuracy in reproducing all details.

Event generation for our simulation was taken from the output of external codes, and these, being relevant to the physics interpretation, will be discussed in detail in the second part of this work [6]. Here we only discuss the quality of the simulation of the detector response.

Event output is produced as an event buffer similar to the real data in order to analyze it with the same offline chain.

All physical processes which are relevant for high energy muons have been activated in the simulation (the residual energy of underground muons has a spectrum with a tail in the TeV range). As discussed in Sec. II A, the tracking performance in the streamer tube digital readout is related to the distribution of the cluster width, which in turn is affected by different processes: the natural width of the induced charge distribution on the pickup strips, the electronics performance, catastrophic energy losses of muons, and δ -ray production. These are known to be very important to reproduce the tails of cluster distribution in gaseous detectors. This can be reliably taken into account by keeping the energy cut for secondary electrons (and photons) at low values. We found that $E_{\text{cut}} = 500$ keV for both secondary electrons and photons matches the required accuracy.

The induction of the streamer charge on the strips has been parametrized with a four-step algorithm. First, the number of streamers for each crossing is estimated according to the track projection along the wire. Then the charge picked up in the wire and induced in the strip plane from each streamer is simulated using the experimental charge distribution. Finally, the charges picked up in the same wires and strips are merged after the tracking of all the particles in the same event. A threshold is then applied in order to reproduce the average readout performance, which also includes some crosstalk effects.

To simulate different run conditions, the code accounts for inefficiencies: at the level of single streamer generation,

in order to reproduce the operating conditions fixed by the gas mixture and anode voltage; at the level of digitization of wire and strip view, in order to reproduce the electronics performance.

The code also includes random uncorrelated hits, that simulate the background due to natural radioactivity. More important for the purpose of multiple muon simulation are noise and crosstalk effects correlated with the number of tracks and possible muon interactions inside the detector, or nearby. These effects have been experimentally studied: they increase both the number of *off-track* hits and the cluster size for events with many muons with respect to the case of single or isolated muon tracks. This is relevant for the track finding, and introduces inefficiencies and ambiguities in the number of tracks reconstructed in the wire and strip views. Therefore, the level of off-track hits correlated with the number of tracks has been parametrized from the experimental data, and it has been added at simulation level after the full GEANT tracking of the events. This addition was found to be successful to obtain the required accuracy in the simulated data. This may be seen in Fig. 2, where for fixed number of tracks reconstructed in the wire view, the average multiplicity in the strip view of the real data are superimposed to those obtained in the simulation.

The reliability of this detector simulation has allowed a substantial improvement of data analysis compared to the procedures described in the early works of MACRO [3], since it allows a drastic reduction of the use of visual event scanning, which is unfeasible for large statistics studies.

Let us define “detected multiplicity” as the number of muons crossing at least four different horizontal planes of the detector. This number is smaller than or equal to the multiplicity of the full underground event. The experimental information in MACRO is given by the measured wire and strip multiplicities. The same “detected multiplicity” can give different pairs of wire and strip multiplicity values, not only because of the different possible spatial configurations of the event, but also because of the features of the detector response. Furthermore, muon interactions, like e.m. showering, can confuse the pattern recognition algorithm when tracks are close together in a projective view. Thus, an event with a “detected multiplicity” N_μ can be reconstructed with m and n tracks in the wire and strip views, respectively. In a fraction of cases, m and/or n are different from N_μ .

If the detector features and muon interactions are accurately modeled, as we claim they are, thanks to our simulation tools, we can use simulated data to obtain on a statistical basis, through an inverse matrix algorithm, the detected muon multiplicity distribution from the set of values of detected wire and strip multiplicities. In detail, we have performed the following steps. By using the Monte Carlo, we estimated the probability $P_{N_\mu}^{n,m}$ that a pair of experimental wire (n) and strip (m) multiplicities is originated by the detected muon multiplicity N_μ as

$$P_{N_\mu}^{n,m} = \frac{M_{N_\mu}^{n,m}}{\sum_i M_i^{n,m}}, \quad (3.1)$$

where $M_{N_\mu}^{n,m}$ ($M_i^{n,m}$) is the number of simulated events with detected muon multiplicity N_μ (i) reconstructed by the track

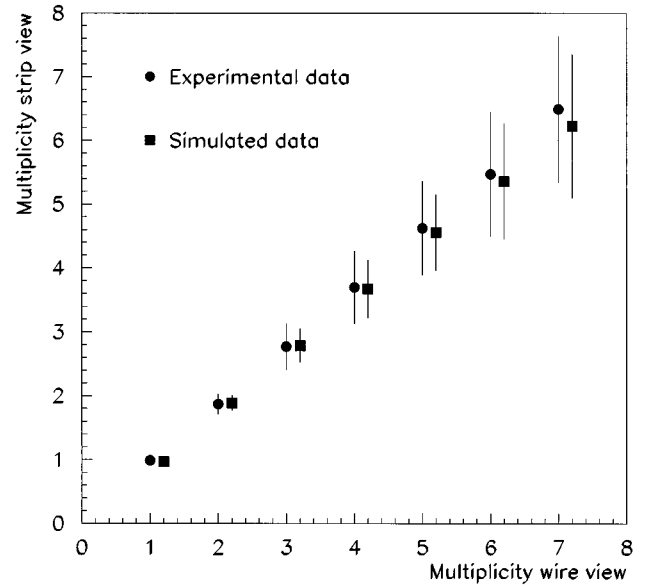


FIG. 2. Comparison of the experimental and simulated averages and rms's of the strip multiplicity distributions at fixed wire multiplicity. The simulated data are slightly shifted to the right for graphical purposes.

finding algorithm with multiplicities m and n in the two views. Therefore, the expected number \mathcal{N}_{N_μ} of events having “detected multiplicity” N_μ can be evaluated using the formula

$$\mathcal{N}_{N_\mu} = \sum_{n,m} P_{N_\mu}^{n,m} \mathcal{M}_{n,m}, \quad (3.2)$$

where $\mathcal{M}_{n,m}$ are the number of reconstructed experimental events with multiplicities n and m in the two views, respectively.

We checked that the systematic uncertainties of the estimated weights are negligible and in particular they do not depend on the chemical composition model used in the Monte Carlo [9] to generate the multiple muon events (see [6]). In Fig. 3 a comparison of two distributions of multiplicity obtained using the same sample of experimental data and two sets of weights estimated from very different chemical composition models (“heavy” and “light” [10]) is shown. No significant differences are visible. We found that this method of evaluating the muon multiplicity is reliable up to $N_\mu \simeq 15$ and a different technique must be used for larger multiplicities as discussed in Sec. V A.

IV. CHARACTERISTICS OF THE GRAN SASSO ROCK

The simulation and reconstruction packages adopted in MACRO include a description of the rock overburden as a function of angular direction.

The rock thickness for a given direction has been obtained from the digitization of the mountain topographic map supplied by the Italian Military Geographical Institute (IGM). Details on the thickness accuracy are given in the Appendix of Ref. [5]; it is at the level of a few percent when small angular windows corresponding to unreliable regions of the topographic map are excluded. This has relevance only for

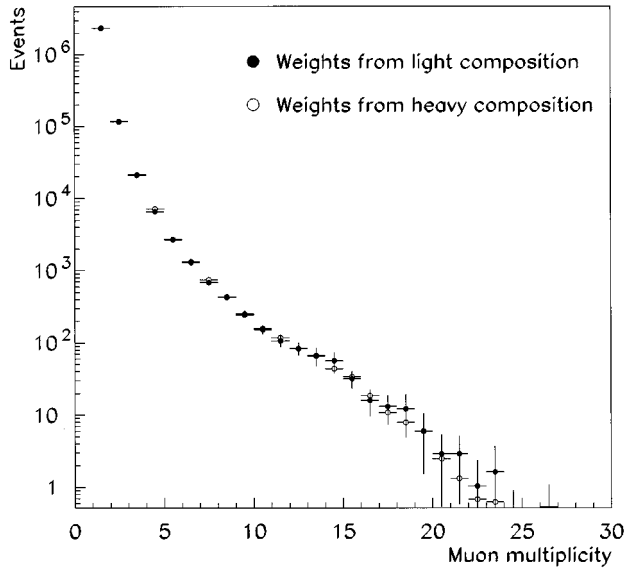


FIG. 3. Multiplicity distribution calculated using the same set of experimental data and two different sets of weights.

the absolute flux measurement.

The structure of the rock overburden surrounding the Gran Sasso underground laboratory is quite irregular; it is essentially calcareous, mixed with other materials, such as aluminium, silicon, magnesium and organic compounds. We made detailed analyses from core samples taken during the tunnel excavation to study the rock structure, and to make a composition and density model of the Gran Sasso rock [11]. The chemical composition results are shown in Table I. The average values of the elemental composition parameters were calculated in the angular range $0^\circ - 60^\circ$; they are very close to the standard rock values (see Table II). However, whenever a conversion to standard rock is requested, we make use of the correction procedure described in Ref. [12], which is a function of density, $\langle Z/A \rangle$ and $\langle Z^2/A \rangle$. The overall resulting uncertainty on the simulation of muon flux underground is less than 5%, as obtained from the 1% uncertainty in the analysis of the depth-intensity function [5].

V. EXPERIMENTAL MEASUREMENTS

As emphasized in the Introduction, it is important to consider all measurements relevant to the physics of high energy

TABLE I. Gran Sasso rock chemical composition [11].

Rock type	Chemical composition	% weight
Limestone	CaCO ₃ (90%), MgCO ₃ (10%)	50
Dolomite limestone	CaCO ₃ (50%), MgCO ₃ (50%)	29
Flint limestone	CaCO ₃ (72%), SiO ₂ (8%), Si, Al, K compounds (20%)	8
Karst formation	CaCO ₃	9
Detritus	CaCO ₃ (49%), MgCO ₃ (1%), Si, Al, K compounds (50%)	3

cosmic rays which can provide information on the energy spectrum, chemical composition, and high energy hadronic interactions. We discuss in one subsection the muon multiplicity distribution, which is the most relevant item for the composition analysis. Other complementary results, in different subsections, are the inclusive muon flux, the angular distribution, and the muon decoherence.

These results have excellent statistical accuracy, so their interpretation is limited by the systematics of the interaction models used in our analysis. We will demonstrate below that systematic uncertainties introduced by the detector are well understood.

A. Muon multiplicity

For each recorded event, DREAM, the MACRO reconstruction program, calculates the track parameters in the projected (*wire* and *strip*) views, unless the complexity of the event prevents a successful reconstruction on both projections. The events rejected for this reason (“rejected data”) are visually analyzed with the aid of an event display program. For successfully reconstructed events, the multiplicities n of *wire tracks* and m of *strip tracks* are used as input to determine the distribution of the “detected muon multiplicity” \mathcal{N}_{N_μ} according to Eq. (3.2) in Sec. III. The variance of the number \mathcal{N}_{N_μ} is

$$\sigma_{N_\mu}^2 = \sum_{n,m} [\sigma_{P_{N_\mu}^{n,m}}^2 \mathcal{M}_{n,m}^2 + (P_{N_\mu}^{n,m})^2 \mathcal{M}_{n,m}], \quad (5.1)$$

where $\sigma_{P_{N_\mu}^{n,m}}$ are the errors on the weights arising from the Monte Carlo simulation.

TABLE II. Gran Sasso rock average parameters. They are very similar to the so-called standard rock for which $A=22$, $Z=11$, and the density = 2.65 g cm^{-3} .

$A=22.87$	$Z=11.41$	Density = $(2.71 \pm 0.05) \text{ g cm}^{-3}$	
Chemical element	Atomic No.	Atomic weight	Relative weight
Hydrogen	1	1.008	0.03
Carbon	6	12.011	12.17
Oxygen	8	15.99	50.77
Magnesium	12	24.305	8.32
Aluminium	13	26.981	0.63
Silicon	14	28.085	1.05
Potassium	19	39.098	0.10
Calcium	20	40.078	26.89

The capability of obtaining an unbiased reconstruction of the multiplicity distribution in the detector has been evaluated from a sample of simulated events. We have generated a set of multiple muon events folded with the detector, recording the distribution of the “detectable multiplicity” (defined as the actual number of muons producing at least four hits in the horizontal planes on each view). We have then compared this distribution to that of “detected multiplicity,” obtained from the processing of simulated data and their reconstruction through the use of Eq. (3.2). To avoid undesired correlations, the simulated data sample used for this purpose is independent of the one used to calculate the weight parameters $P_{N_\mu}^{n,m}$. The distribution of the reconstructed “detected multiplicity” turns out to coincide, within the statistical error, with the distribution of “detectable multiplicity” for all the events for which the tracking algorithm is successful (i.e., provides at least one reconstructed muon), up to $N_\mu = 15$. For larger values, the ratio of the two distribution departs from unity, and drops linearly with N_μ , vanishing at about 32 muons. This ratio is used to provide a linear correction function.

Figure 4 shows the multiplicity distribution of reconstructed events obtained using formula (3.2) (open circles) and the one obtained after accounting for the above-described correction function for the track reconstruction capability (full circles).

Events belonging to the “rejected data sample” were visually scanned by two independent groups. The whole sample of rejected events consisted of 2321 events, to be compared with ~ 4.4 million reconstructed events. Of these events, 129 were recognized as genuine high multiplicity muon events whereas the rest were discarded as being due to electronic noise fluctuations in the streamer tube system. We assigned a range of different multiplicities to events when the true multiplicity could not be unambiguously determined (mainly high density events with several muons or with showers). This was done giving an equal fractional weight to each possible multiplicity within the range defined by the scanners. To give an example of the uncertainty achievable in the visual scanning, in the range around $N_\mu = 20$, we obtain a $\sigma_{N_\mu} = 1.2$. Such value smoothly rises up to 2.5 above $N_\mu = 35$. The event with the highest multiplicity has obtained from the scanning $N_\mu = 41$, with an uncertainty $\sigma_{N_\mu} = 4$.

In Fig. 4 the multiplicity distribution of the scanned events is given by open squares. The systematic error on this sample, evaluated on the basis of the double scanning, is small with respect to the statistical one. We show data up to $N_\mu = 39$.

The same scanning procedure has also been applied on a sample of simulated events, roughly the same statistical size as the real data which were rejected by the tracking algorithm. A comparison of the “detectable multiplicity” with the one (or the multiplicity interval) assigned by the scanners showed that the assigned multiplicity is systematically underestimated. This fact is to be attributed to a limit of the detector resolution when the track density is high enough to obscure muon tracks (especially in presence of showering activity) and thus to prevent the discrimination of individual tracks. This systematic effect is small for less than 25 muons, but becomes important above 30 muons. An unfolding pro-

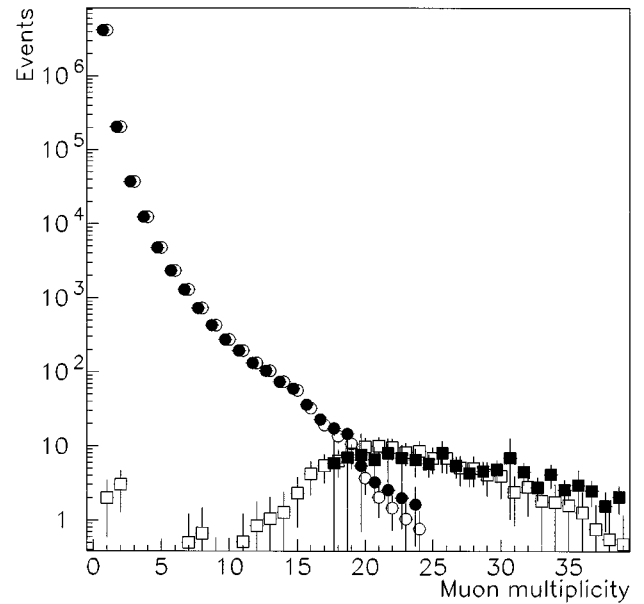


FIG. 4. Muon multiplicity distributions for the data samples of reconstructed events (circles) and scanned events (squares). The open circles refer to the distribution obtained according to formula (3.2) in the text. The application of the correction function for $N_\mu \geq 15$ (described in the text) gives rise to the distribution with full circles. The multiplicity distribution obtained through a visual scanning of the data sample rejected by the reconstruction program is plotted with open squares. Full squares show the distribution arising from the unfolding of this data sample (see text). The data points have abscissae slightly shifted for graphical purposes.

cedure based on the Bayes’ theorem [14] has been applied to account for this effect; it uses the correlation between the “detectable multiplicity” and the scanned multiplicity from the sample of simulated events. Alternative unfolding methods used for comparison give similar results. The Bayes’ method, however, produces a correct (and theoretically well grounded) evaluation of the unfolding uncertainties. Figure 4 shows the multiplicity distribution of the unfolded scanned events with full squares.

The corrected muon rates, obtained by merging the reconstructed muon sample with the unfolded muon sample, are shown in Fig. 5 and reported in Table III. A systematic error (evaluated by a comparison with Monte Carlo simulation) of 20% has been added in quadrature for $N_\mu \geq 15$ to account for uncertainties in the merging between the two data samples.

We stress that such a distribution is that of the muons detected in MACRO, and it is, in principle, different from the one measurable by any other different detector, even if located at the same site, since it is affected by the detector acceptance. We have also studied the possibility of unfolding a multiplicity distribution as seen from a detector with “infinite area,” as attempted by the Frejus experiment [15]. We have concluded that it is not possible to achieve an unbiased results, for two reasons: (1) an unfolding procedure, like the one proposed in [15], depends on the assumption on the lateral distribution function of muons, which is also found to be dependent on the composition model, although to a smaller extent than the multiplicity distribution; (2) the same unfold-

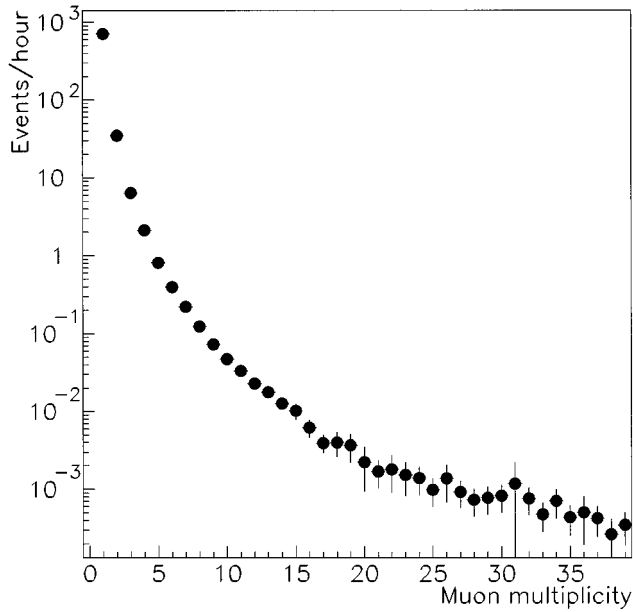


FIG. 5. Muon rates at different multiplicities in events/h.

ing procedure requires that multiple muon events are fully reconstructed in space. This requires an unambiguous spatial association of the tracks from the two projective views, but the efficiency to achieve such association in MACRO is found to drop with increasing values of N_μ . This is the major problem preventing a successful unfolding.

B. Complementary measurements on underground muons

The data collected by underground experiments strongly depend on the structure and characteristics of the rock overburden and on the performance of the detector. In order to compare different experiments, detector independent physical results must be unfolded from the data by means of a detailed understanding of the detector response and of a good knowledge of the overburden rock and of its chemical composition, summarized in Sec. IV. The inclusive muon flux, commonly expressed through the vertical muon intensity as a

function of the rock slant depth crossed by the muons, is a detector-independent measurement which allows a comparison with other experiments. Moreover, it also provides an indirect comparison to the measurement of muon flux in atmosphere.

This kind of analysis, performed with the MACRO detector on a sample of more than 3×10^6 muons in the zenith angular range $0^\circ - 60^\circ$ (for a rock overburden between 3000 and 7000 hg/cm^{-2}) is described in detail in [5]. Here we review the fundamental results.

The vertical muon intensity is defined as

$$I(h) = \left(\frac{1}{\Delta T} \right) \left\langle \frac{\sum_i N_i m_i}{\sum_j \Delta \Omega_j A_j \epsilon_j / \cos \theta_j} \right\rangle, \quad (5.2)$$

where ΔT is the live time, N_i is the number of observed events of muon multiplicity m_i in the angular bin $\Delta \Omega_j$ of slant depth h , $A_j(\theta, \phi)$ is the detector projected area for that bin, $\epsilon_j(\theta, \phi)$ is the combined trigger and reconstruction efficiency; θ and ϕ are the muon zenith and azimuth angles. The average is performed over the angles at fixed slant depth h . The two matrices A_j and ϵ_j were calculated with an accuracy better than 1% using the detector simulation package, where the precise geometry and all the inefficiency sources were included. In Fig. 6, the MACRO vertical muon intensity is shown together with a world compilation of the results of the main experiments [15–22].

The good quality of the MACRO data fixes the uncertainties resulting from the previous measurements. In addition, the overall agreement between MACRO data and the world compilation ensures that, at a few percent level, both detector response and data treatment are under very good control. Also, topological or chemical systematics associated with the overburden rock is ruled out at the same accuracy level. This conclusion is relevant to the primary cosmic ray composition analysis, since it constrains systematic uncertainties in the rock overburden, and gives us confidence on the measurements of absolute fluxes.

In Ref. [5], MACRO has already shown that, up to a zenith angle of 60° , the inclusive flux of atmospheric cosmic

TABLE III. Muon rates at different multiplicities in events/h (see text).

N_μ	Rate	N_μ	Rate	N_μ	Rate
1	712.1 ± 0.8	14	$(1.3 \pm 0.1) \times 10^{-2}$	27	$(9 \pm 4) \times 10^{-4}$
2	34.7 ± 0.4	15	$(1.0 \pm 0.2) \times 10^{-2}$	28	$(7 \pm 3) \times 10^{-4}$
3	6.35 ± 0.08	16	$(6.2 \pm 1.6) \times 10^{-3}$	29	$(8 \pm 3) \times 10^{-4}$
4	2.11 ± 0.09	17	$(3.9 \pm 1.0) \times 10^{-3}$	30	$(8 \pm 3) \times 10^{-4}$
5	$(8.11 \pm 0.19) \times 10^{-1}$	18	$(4.0 \pm 1.4) \times 10^{-3}$	31	$(1 \pm 1) \times 10^{-3}$
6	$(3.96 \pm 0.11) \times 10^{-1}$	19	$(3.7 \pm 1.5) \times 10^{-3}$	32	$(8 \pm 3) \times 10^{-4}$
7	$(2.21 \pm 0.08) \times 10^{-1}$	20	$(2.2 \pm 1.3) \times 10^{-3}$	33	$(5 \pm 2) \times 10^{-4}$
8	$(1.24 \pm 0.05) \times 10^{-1}$	21	$(1.7 \pm 0.6) \times 10^{-3}$	34	$(7 \pm 3) \times 10^{-4}$
9	$(7.3 \pm 0.4) \times 10^{-2}$	22	$(1.8 \pm 0.9) \times 10^{-3}$	35	$(4 \pm 2) \times 10^{-4}$
10	$(4.7 \pm 0.3) \times 10^{-2}$	23	$(1.5 \pm 0.7) \times 10^{-3}$	36	$(5 \pm 3) \times 10^{-4}$
11	$(3.3 \pm 0.2) \times 10^{-2}$	24	$(1.4 \pm 0.6) \times 10^{-3}$	37	$(4 \pm 2) \times 10^{-4}$
12	$(2.3 \pm 0.2) \times 10^{-2}$	25	$(1.0 \pm 0.4) \times 10^{-3}$	38	$(3 \pm 2) \times 10^{-4}$
13	$(1.8 \pm 0.2) \times 10^{-2}$	26	$(1.4 \pm 0.7) \times 10^{-3}$	39	$(4 \pm 2) \times 10^{-4}$

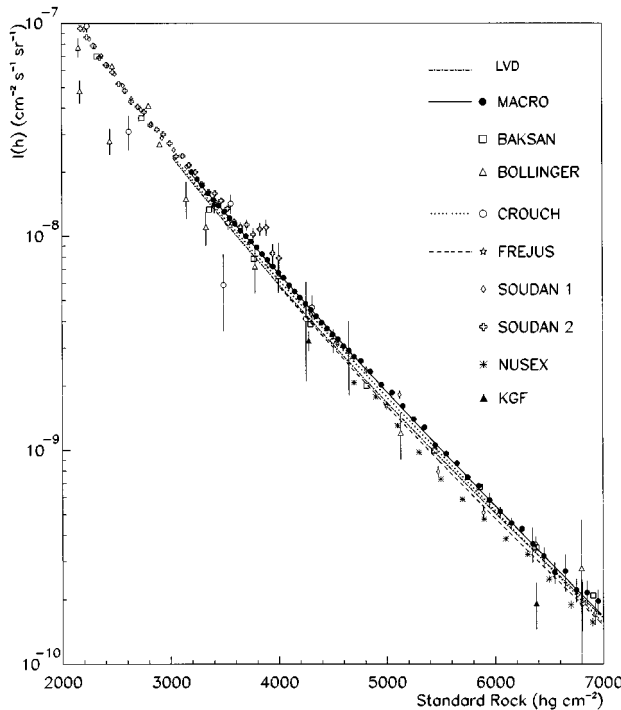


FIG. 6. Vertical muon intensity vs standard rock as measured by MACRO [5], the data compiled by Crouch [16], and those obtained by other experiments: LVD [17], Baksan [18], Bollinger [19], Frejus [15], Soudan 1 and Soudan 2 [20], NUSEX [21], KGF [22]. The solid line is the fit of our data; the dotted line is the Crouch fit [16]; the dashed line is the Frejus fit. Notice that the LVD measurement has been performed using single muon events only.

muons in the TeV range has an angular dependence consistent with a $\sec(\theta)$ law. We emphasize that the zenith and azimuthal angular distribution of high energy muons detected underground is strongly dependent on the rock overburden, due to the angle-depth correlation introduced by the mountain profile. The detector acceptance also has angular dependence. It can be expected that events with different multiplicity might exhibit a different zenith angle dependence with respect to that of the inclusive flux. In Fig. 7 we show the zenith angle distribution of events with detected multiplicity $N_\mu=2,3,4$ as compared to the Monte Carlo prediction [9]. The agreement between data and simulation is reasonably good and is mainly limited by the systematics in our knowledge of the rock. This uncertainty does not allow us, for the moment, to draw firm conclusions on the possible dependence on multiplicity.

The decoherence function (frequency of all possible pairs of muons as a function of distance between them) is primarily sensitive to energy, transverse momentum distribution, and production height of parent mesons (i.e., to the primary hadronic interaction) and to muon multiple scattering in the rock. This distribution is weakly dependent on primary composition. Therefore, we consider understanding the muon decoherence function an essential step before attempting any analysis of the muon multiplicity distribution in terms of primary composition. The reason is that the transverse structure of the showers has to be well reproduced by the inter-

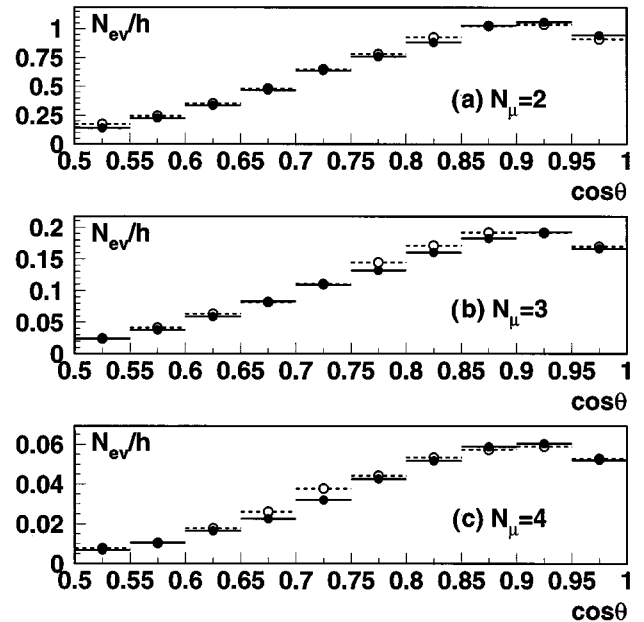


FIG. 7. Distribution in cosine of the zenith angle of the event rate detected in MACRO for muon multiplicity 2 (a), 3 (b), and 4 (c), compared to Monte Carlo predictions. Full circles are experimental data, while open symbols are simulation results.

action model adopted in the analysis, since it affects the simulation of the muon multiplicity distribution in a finite size detector.

The capability of MACRO to measure muon pair separation is based on the pattern recognition algorithm's ability to associate unambiguously the tracks of both projective views in a large fraction of cases. Figure 8 shows the measured decoherence distribution as obtained from the detected multimoon event sample (full symbols), in the form dN/DD^2 , D being the muon pair separation. Monte Carlo predictions of these decoherence results, an important crosscheck, will be discussed in part II of this work.

The decoherence measured by a finite-size detector is biased by detector's dimensions. Pair separation that exceeds the detector's dimensions clearly cannot be measured, nor can separations less than the detector spatial resolution. A detector-independent decoherence function can be unfolded from the measured one, for the pair distance range allowed by the apparatus, provided that the detector geometry and efficiency are properly considered in track reconstruction of the penetrating particles. A description of two unfolding methods adopted in MACRO is given in [4], where the results using data taken with the first two supermodules were used. The first decoherence results obtained with all six supermodules were presented in [23] and are shown in Fig. 8 (open symbols), with an arbitrary scale.

The results shown so far are statistically dominated by double muon events. However, there can be some interest in measuring the muon pair separation for different ranges of detected multiplicities. The reason is twofold: (1) There exists a dependence between the detected number of muons and the primary energy, and the evolution with energy of $\langle P_\perp / h_{\text{prod}} \rangle$ of parent mesons (h_{prod} being the production height) influences the decoherence curve; (2) the multiplicity

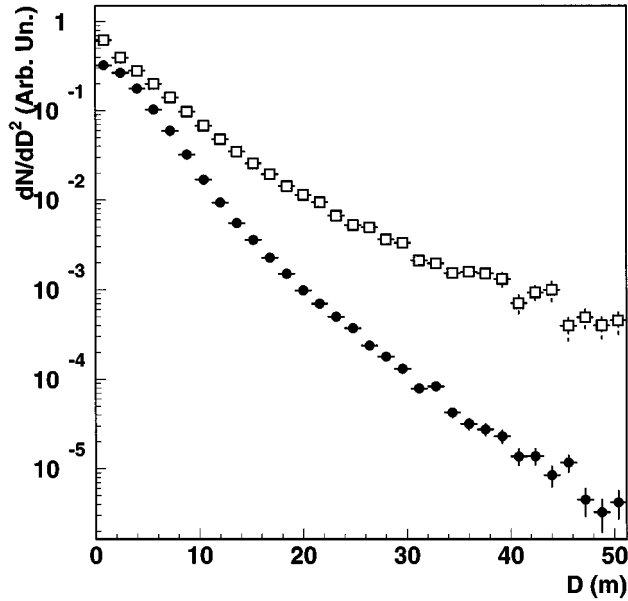


FIG. 8. Muon decoherence distribution (full symbols) as measured in the MACRO detector. The distribution with the open symbols is the result after the unfolding of the detector acceptance, as presented in [23]. Here, each muon pair enters with a $1/N_{\text{pair}}$ weight, where N_{pair} is the number of unambiguously reconstructed pairs.

selection can introduce a significant composition dependence on the decoherence curve, since nuclei heavier than protons, if present, produce a greater average muon multiplicity, and give larger contributions to the decoherence curve [24].

From the experimental point of view, a decoherence analysis at high multiplicity can be done without bias by MACRO only by considering the muon separation projected in one view. Otherwise, as already mentioned in Sec. V A, the requirement of an unambiguous spatial association would artificially deplete the large N_{μ} event sample. In Fig. 9 we show the decoherence distribution projected on the wire view for events with multiplicities $N_{\mu}=2$, $N_{\mu}=4-6$, and $N_{\mu}=7-20$. It can be noticed how the average value of separation tends to decrease with increasing multiplicity. This is expected, since larger multiplicities are correlated to higher energies. In practice, from these plots it is understandable how the average spatial density of muons increases with multiplicity. Neglecting these small differences, about 64% of muons falls within a circle with radius of 6 m. The resulting effect on projective views, where tracks may superimpose one to another, explains the decreasing efficiency in pattern recognition for large detected multiplicities.

In the second part of this work, we discuss the results on the projected muon decoherence for different multiplicities in terms of the composition model.

The relative angles and distances of muon pairs must be correlated through the properties of primary interaction, such as the total cross section and the transverse momentum distribution. In the case of muons detected underground, the effect of muon scattering hides such a functional dependence between angle and distance.

However, the underlying physics remains contained in the double differential distribution of muon pair flux with re-

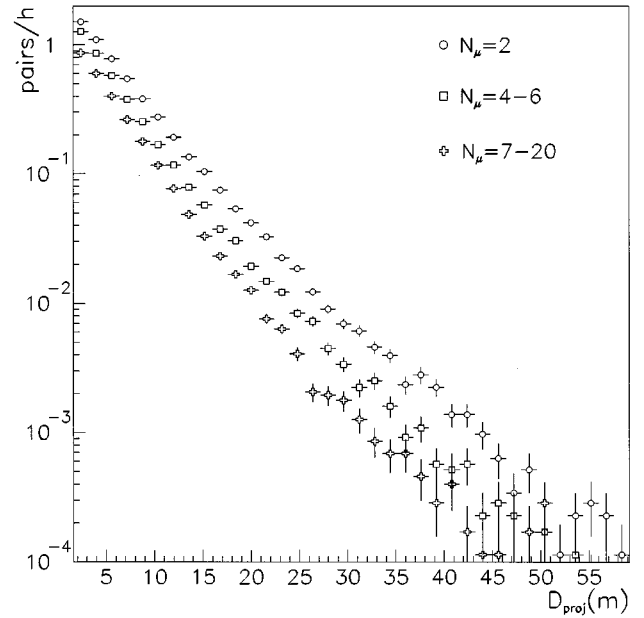


FIG. 9. The experimental muon lateral separation projected in the wire view for different event multiplicities. Here, each muon pair enters with unit weight.

spect to their relative angle and distance: the decoherence is a quantity related to the zeroth moment of the distribution with respect to the angle. In order to extract as much physical information as possible, other measurements are conceivable. In particular, it has been proposed [13] that the ‘‘decorrelation function,’’ i.e., the relative average angle between muon pairs in a bundle, is a sensitive tool to study the physics related to both the interaction model and the muon propagation, in addition to the more traditional decoherence measurement. The experimental measurement of the decorrelation function will be the subject of a future dedicated paper by MACRO.

VI. CONCLUDING REMARKS

We have shown that the reconstruction and analysis of muon events in MACRO is well controlled. The systematics due to detector effects and analysis algorithms are well understood and can be reliably corrected. The statistical accuracy achieved by MACRO would now be sufficient, in principle, to reach definite physics conclusions for primary composition. The remaining uncertainties in the analyses of high energy cosmic ray physics (described in part II of this work) will be largely dominated by those related in the interaction models.

ACKNOWLEDGMENTS

We gratefully acknowledge the Istituto Nazionale di Fisica Nucleare, the Laboratori Nazionali del Gran Sasso and its staff, the U.S. Department of Energy, the U.S. National Science Foundation, for their generous support of the MACRO experiment. The continuous and precious support of our technicians was essential to assure the quality of data taking.

- [1] T. K. Gaisser and T. Stanev, Nucl. Instrum. Methods Phys. Res. A **235**, 183 (1983).
- [2] MACRO Collaboration, S. P. Ahlen *et al.*, Nucl. Instrum. Methods Phys. Res. A **324**, 337 (1993).
- [3] MACRO Collaboration, S. P. Ahlen *et al.*, Phys. Rev. D **46**, 895 (1992).
- [4] MACRO Collaboration, S. P. Ahlen *et al.*, Phys. Rev. D **46**, 4836 (1992).
- [5] MACRO Collaboration, M. Ambrosio *et al.*, Phys. Rev. D **52**, 3793 (1995).
- [6] MACRO Collaboration M. Ambrosio *et al.*, following paper, Phys. Rev. D **56**, 1418 (1997).
- [7] MACRO Collaboration, S. P. Ahlen *et al.*, Astrophys. J. **412**, 301 (1993).
- [8] R. Brun *et al.*, CERN Report No. DD/EE/84-1, 1992 (unpublished).
- [9] C. Forti *et al.*, Phys. Rev. D **42**, 3668 (1990).
- [10] G. Auriemma *et al.*, *Proceedings of 21st International Cosmic Ray Conference*, Adelaide, Australia, 1990, edited by R. J. Protheroe (Graphic Services, Northfield, South Australia, 1990), Vol. 9, p. 362.
- [11] P. G. Catalano *et al.*, Mem. Soc. Geol. Ital. **35**, 647 (1986).
- [12] A. G. Wright, *Proceedings of 12th International Cosmic Ray Conference*, Denver, 1973 (University of Denver, Denver, 1973), Vol. 3, p. 1709.
- [13] A. F. Grillo and S. Parlati, Astropart. Phys. **2**, 335 (1994).
- [14] G. D'Agostini, Nucl. Instrum. Methods Phys. Res. A **362**, 487 (1995).
- [15] Ch. Berger *et al.*, Phys. Rev. D **40**, 2163 (1989).
- [16] M. Crouch, in *Proceedings of 20th International Cosmic Ray Conference*, Moscow, USSR, 1987, edited by V. L. Kozaryivsky *et al.* (NAUKA, Moscow, 1987), Vol. 6, p. 165.
- [17] LVD Collaboration, M. Aglietta *et al.*, Astropart. Phys. **3**, 311 (1995).
- [18] Y. M. Andreyev, V. I. Gurentsov, and I. M. Kogai, *Proceedings of 20th International Cosmic Ray Conference* [16], Vol. 6, p. 200.
- [19] L. M. Bollinger, Phys. Rev. **79**, 207 (1950).
- [20] K. Ruddick (private communication); Soudan Collaboration, Report No. PDK-435, 1990 (unpublished); S. M. Kasahara, Ph.D. thesis, University of Minnesota, 1995.
- [21] M. Aglietta *et al.*, Nuovo Cimento C **9**, 196 (1986); in *Astrophysics and Particle Physics*, Proceedings of the Topical Seminar, San Miniato, Italy, 1989, edited by F. T. Navarra and P. G. Pelfer [Nucl. Phys. B (Proc. Suppl.) **14**, 193 (1990)].
- [22] M. G. K. Menon and P. V. Ramana Murthy, Prog. Elem. Part. Cosm. Ray Phys. **IX**, 163 (1967).
- [23] The MACRO Collaboration, S. P. Ahlen *et al.*, *Proceedings of the 23rd International Cosmic Ray Conference*, Calgary, Canada, 1993, edited by R. B. Hicks *et al.* (World Scientific, Singapore, 1994), Vol. 2, p. 93.
- [24] J. W. Elbert, Phys. Rev. D **27**, 1448 (1983).